INTERNATIONAL JOURNAL FOR NUMERICAL METHODS IN ENGINEERING
Int. J. Numer. Meth. Engng 2001; **51**:275–292

Displacement/pressure mixed interpolation in the method of finite spheres

Suvranu De and Klaus-Jürgen Bathe*,†

Department of Mechanical Engineering, Massachusetts Institute of Technology, 77 Massachusetts Avenue, Cambridge, MA 02139, U.S.A.

SUMMARY

The displacement-based formulation of the method of finite spheres is observed to exhibit volumetric 'locking' when incompressible or nearly incompressible deformations are encountered. In this paper, we present a displacement/pressure mixed formulation as a solution to this problem. We analyse the stability and optimality of the formulation for several discretization schemes using numerical inf–sup tests. Issues concerning computational efficiency are also discussed. Copyright © 2001 John Wiley & Sons, Ltd.

KEY WORDS: method of finite spheres; meshless technique; incompressible analysis

1. INTRODUCTION

Earlier we introduced a truly meshless numerical scheme—the method of finite spheres—for the solution of boundary value problems on complex domains [1]. In this technique the discretization is performed using functions that are compactly supported on general *n*-dimensional spheres and the Galerkin weak form of the governing differential equations is integrated using specialized numerical integration rules.

We noted, however, that while complex problems could be solved using the method of finite spheres, the method is not as efficient as the traditional finite element techniques. The issue of efficiency is clearly of primary importance. While many apparently different meshless techniques have been proposed in the literature, the ultimate utility of a meshless method depends on whether it is reasonably efficient when compared with the now classical finite element procedures. It is for this reason that we have focused on the issues of efficiency and reliability. In this respect, it need also be noted that the displacement-based method of finite spheres exhibits, of course, volumetric locking in almost or fully incompressible deformations. The purpose of this paper is to investigate these issues in greater detail.

*Correspondence to: Klaus-Jürgen Bathe, Department of Mechanical Engineering, Massachusetts Institute of Technology, Room 3-356, 77 Massachusetts Avenue, Cambridge, MA 02139, U.S.A.
†E-mail: kjb@mit.edu

Received 5 June 2000
Revised 9 August 2000

Copyright © 2001 John Wiley & Sons, Ltd.

It is well known that the solution of almost incompressible elasticity problems using the standard displacement-based finite element technique and reasonable meshes may yield solutions that are grossly in error [2]. The difficulty is that the computed displacement field needs to satisfy the constraint of very small volumetric strains (which become zero as the condition of total incompressibility is approached) while the pressure is of the order of the boundary tractions. The displacement approximation space is not rich enough to accommodate this constraint without a drastic reduction in the rate of convergence, a condition referred to as 'locking' [2].

For the analysis of such problems, it is necessary to use a mixed formulation [2] in which separate approximation spaces are used for the displacement and pressure fields. While, in principle, numerous mixed formulations may be developed, only those that are stable are useful in practice. The solvability, stability and optimality of mixed formulations are expressed in the ellipticity requirement and the inf–sup condition [2]. The ellipticity condition is relatively easy to satisfy. The analytical proof whether the inf–sup condition is satisfied for a specific formulation is, however, difficult. Hence, a numerical inf–sup test was designed [2, 3].

Over the past decade, several meshless techniques have been proposed but the issue of locking has not been studied in depth. Until recently, it was stated that meshfree methods are immune to locking. Indeed it was reported that the element free Galerkin method has the advantage that it does not suffer from locking [4–7]. Furthermore, the element free Galerkin method has been actually proposed as a solution to the locking problem in isochoric elasto-plastic analyses especially when a sufficiently large support size for the interpolation functions is chosen [8].

In the context of another meshless scheme, the reproducing kernel particle method, a similar claim was made confirming the absence of volumetric locking when analysing large deformation behaviour of nearly incompressible hyperelastic materials [9]. More recently, Li and Liu [10] have reported that they have been able to simulate shear band formation successfully in inelastic solids using an explicit displacement-based formulation and the reproducing kernel particle method. They have linked the absence of locking to the choice of higher order polynomial interpolation and the use of reduced order integration. In these publications, the conclusions were drawn primarily by only studying the analysis results of a few example problems and not considering the inf–sup condition.

Only recently, it has been reported that the element-free Galerkin method does indeed suffer from locking in incompressible deformations [11]. The locking is pronounced when moving least-squares interpolants with small support size are used. Functions with small support size are necessary in practice for better localization and a lower bandwidth of the system matrices. In their paper, Dolbow and Belytschko [11] have proposed a mixed displacement/pressure formulation and selective reduced integration to alleviate locking. However, with a linear displacement field and a constant pressure field, the scheme does not pass the numerical inf–sup test. Chen *et al*. note that the use of large support size is computationally expensive and, moreover, cannot remove pressure oscillations [12, 13]. They propose a pressure projection method to remove locking and pressure oscillations in nearly incompressible finite elasticity problems together with a reduced integration scheme. No inf–sup tests were however performed to test the stability of the proposed scheme.

In this paper we present a mixed displacement/pressure formulation as a remedy to the problem of locking encountered in incompressible deformations and analyse the stability and optimality of several displacement/pressure discretization schemes using a numerical inf–sup

Copyright © 2001 John Wiley & Sons, Ltd.

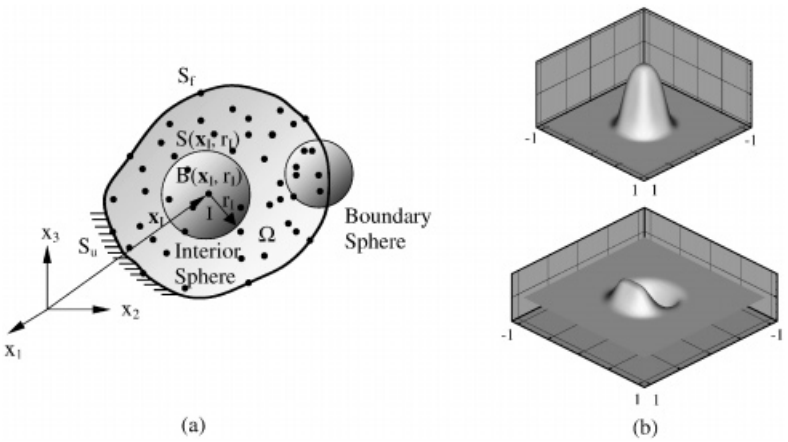

Figure 1. (a) A schematic of the method of finite spheres; and (b) some shape functions in two-dimensions.

test. This numerical inf–sup test is used for mixed formulations like the numerical patch test is used for non-conforming displacement discretizations [3].

The organization of this paper is as follows. In Section 2 we review the interpolation scheme used in the displacement-based method of finite spheres. In Section 3 we introduce a displacement/ pressure mixed formulation for the analysis of problems involving linear elastic solids. In Section 4 we address the important issue of numerical integration and introduce several different integration rules. In Section 5 we discuss the inf–sup condition, introduce a numerical form in the context of the method of finite spheres and analyse the stability of several displacement/pressure discretization schemes.

2. THE INTERPOLATION SCHEME

In this section, we review the specific interpolation scheme used in the displacement-based method of finite spheres [1].

2.1. Shape functions

Let $\Omega \in R^n$ $(n = 1, 2 \text{ or } 3)$ be an open bounded domain and let S be its boundary (see Figure 1). Let a family of open spheres $\{B(\mathbf{x}_I, r_I);\ I = 1, 2, \ldots, N\}$ form a covering for Ω, i.e. $\Omega \subset \bigcup_{I=1}^{N} B(\mathbf{x}_I, r_I)$, where $\mathbf{x}_I$ and r_I refer to the centre and radius of the sphere, respectively. We associate a 'node' with the geometric centre of each sphere. By $S(\mathbf{x}_I, r_I)$ we denote the surface of the sphere with centre $\mathbf{x}_I$ and radius r_I. The spheres may be entirely within the domain (interior spheres) or may have non-zero intercepts with the boundary (boundary spheres), see Figure 1.

The interpolation functions are compactly supported on the spheres and are generated using the partition of unity paradigm [14, 15]. The first step is to define, at each node I, a basis

Copyright © 2001 John Wiley & Sons, Ltd.

function, $\varphi_I^0(\mathbf{x})$, satisfying

1. $\sum_{I=1}^{N} \varphi_I^0(\mathbf{x}) = 1 \ \forall \mathbf{x} \in \Omega$.
2. $\text{supp}(\varphi_I^0(\mathbf{x})) \subset B(\mathbf{x}_I, r_I)$.
3. $\varphi_I^0(\mathbf{x}) \in C_0^s(R^n), \ s \geqslant 0$.

This system of functions $\{\varphi_I^0(\mathbf{x})\}_{I=1}^N$ is said to form a *partition of unity* subordinate to the open cover $\{B(\mathbf{x}_I, r_I)\}$.

The functions $\{\varphi_I^0(\mathbf{x})\}$ satisfy zeroth-order consistency, i.e. they ensure that rigid body modes are exactly represented. To attain higher-order consistency, we define at each node I, a local approximation space $V_I^h = \text{span}_{m \in \mathscr{I}}\{p_m(\mathbf{x})\}$, where $p_m(\mathbf{x})$ is a polynomial or other function and $\mathscr{I}$ is an index set. The superscript h is a measure of the size of the spheres.

The global approximation space V_h is generated by multiplying the partition of unity function at each node I with the functions from the local basis

$$V_h = \sum_{I=1}^{N} \varphi_I^0 V_I^h$$

Hence, any function $v_h \in V_h$ can now be written as

$$v_h(\mathbf{x}) = \sum_{I=1}^{N} \sum_{m \in \mathscr{I}} h_{Im}(\mathbf{x}) \alpha_{Im} \tag{1}$$

where

$$h_{Im}(\mathbf{x}) = \varphi_I^0(\mathbf{x}) p_m(\mathbf{x}) \tag{2}$$

and h_{Im} is a basis/shape function associated with the mth degree of freedom α_{Im} of node I. It can be seen that if a function $p_m(\mathbf{x})$ is included in the local basis of all the nodes, then it is possible to exactly reproduce $p_m(\mathbf{x})$ on the entire domain. This is the well-known *reproducing property* of the shape functions.

2.2. Choice of the partition of unity functions

We use a particular family of (nonpolynomial) partition of unity functions, called the Shepard partitions of unity functions [16] defined by

$$\varphi_I^0(\mathbf{x}) = \frac{W_I}{\sum_{J=1}^{N} W_J} \tag{3}$$

where $W_I(\mathbf{x})$ denotes a radial function compactly supported on the sphere centred at node I such that $\text{supp}(W_I) \subset B(\mathbf{x}_I, r_I)$. Important consideration should be given to the choice of the functions $W_I(\mathbf{x})$ so that a low cost partition of unity is obtained. We concentrate on radial functions of the form $W_I(\mathbf{x}) = W(s_I)$, where $s_I = \|\mathbf{x} - \mathbf{x}_I\|_0 / r_I$. The following remarks are useful in the choice of the functional form of W_I:

Remark 2.1. Let $W_I \in C_0^s(B(\mathbf{x}_I, r_I))$, $I = 1, 2, \ldots, N$ and let $p_m(\mathbf{x}) \in C^l(\Omega)$ for $s, l \geqslant 0$; then the shape functions $h_{Im}(\mathbf{x})$ satisfy $h_{Im}(\mathbf{x}) \in C_0^{\min(s,l)}(B(\mathbf{x}_I, r_I) \cap \Omega)$.

The proof is immediate from Equation (2). The following two remarks are direct consequences.

Copyright © 2001 John Wiley & Sons, Ltd.

Remark 2.2 (*Displacement continuity*). The displacement field is continuous so long as the functions W_I and $p_m(\mathbf{x})$ are continuous.

Remark 2.3 (*Stress continuity*). The stress fields, obtained by differentiating the displacement field (1), are continuous on Ω if each of the functions W_I has zero slope at the centre, $\mathbf{x}_I$, and on the surface, $S(\mathbf{x}_I, r_I)$ of the sphere on which it is defined, provided the functions $p_m(\mathbf{x})$ and their derivatives are sufficiently smooth.

The above statement can be understood more clearly if we recognize that, for sufficiently smooth functions $p_m(\mathbf{x})$, the stress fields are continuous provided the derivatives of W_I with respect to the spatial coordinates x_i $(i \in \{1,2,3\})$

$$\frac{\partial W(s_I)}{\partial x_i} = \frac{x_i - x_{Ii}}{r_I^2}\left[\frac{1}{s_I}\frac{\mathrm{d}W(s_I)}{\mathrm{d}s_I}\right] \tag{4}$$

are continuous in $B(\mathbf{x}_I, r_I)$ and on $S(\mathbf{x}_I, r_I)$.

This derivative exists as $s_I \to 0$ if W_I has zero slope at the centre of the sphere. Moreover, the derivative in Equation (4) is continuous on $S(\mathbf{x}_I, r_I)$, i.e. as $s_I \to 1$ if W_I has zero slope on the surface $S(\mathbf{x}_I, r_I)$.

Equation (4) introduces two conditions on the first derivative of the function W_I if a continuous stress field is to be obtained. A third condition arises from the constraint that the function W_I vanishes on $S(\mathbf{x}_I, r_I)$, i.e. $W(s_I = 1) = 0$. To satisfy these three conditions, the function W_I needs to be at least a cubic in s_I. We have, therefore, chosen a cubic spline weight function of the following form:

$$W(s_I) = \begin{cases} \frac{2}{3} - 4s_I^2 + 4s_I^3, & 0 \leqslant s_I < \frac{1}{2} \\ \frac{4}{3} - 4s_I + 4s_I^2 - \frac{4}{3}s_I^3, & \frac{1}{2} < s_I \leqslant 1 \\ 0, & s_I > 1 \end{cases} \tag{5}$$

These cubic spline functions can be used to generate less expensive Shepard functions than the quartic spline functions used in Reference [1].

3. MIXED DISPLACEMENT/PRESURE FORMULATION

In this section, we briefly review the governing equations for a linear elastic continuum in 2D and then derive a displacement/pressure mixed formulation and discretized equations.

3.1. Governing equations

Let us consider an open bounded domain $\Omega \subset R^2$. Let S be its boundary. The system of governing differential equations and the boundary conditions can be written as

Equilibrium equations:

$$\boldsymbol{\partial}_{\varepsilon}^{\mathrm{T}}\boldsymbol{\tau} + \mathbf{f}^B = \mathbf{0} \quad \text{in } \Omega \tag{6}$$

Strain–displacement relationships:

$$\boldsymbol{\varepsilon} = \boldsymbol{\partial}_{\varepsilon}\mathbf{u} \quad \text{in } \Omega \tag{7}$$

Copyright © 2001 John Wiley & Sons, Ltd.

Boundary conditions:

$$\mathbf{N}\boldsymbol{\tau} = \mathbf{f}^S \quad \text{on } S_f \tag{8}$$

$$\mathbf{u} = \mathbf{u}^S \quad \text{on } S_u \tag{9}$$

In Equations (6)–(9), $\mathbf{u}$, $\boldsymbol{\varepsilon}$ and $\boldsymbol{\tau}$ are the displacement, stress and strain vectors, $\mathbf{f}^S$ is the prescribed traction vector on the Neumann boundary S_f, $\mathbf{u}^S$ is the vector of prescribed displacements on the Dirichlet boundary S_u (note that the domain boundary $S = S_f \cup S_u$ and $S_f \cap S_u = \{0\}$), $\mathbf{f}^B$ is the body force vector (including inertia terms), ∂_ε is a linear gradient operator and $\mathbf{N}$ is the matrix of direction cosine components of a unit normal to the domain boundary (positive outwards).

If the body is made of an almost incompressible medium, we anticipate that the volumetric strains will be small compared to the deviatoric strains and write the constitutive relationship in the following form

$$\boldsymbol{\tau} = -p\mathbf{I} + 2G\boldsymbol{\varepsilon}^{\mathrm{D}} \tag{10}$$

where $\mathbf{I}$ is the vector corresponding to the Kronecker delta, G is the shear modulus

$$G = \frac{E}{2(1+v)} \tag{11}$$

where E and v are the Young's modulus and the Poisson ratio of the material, respectively. $\boldsymbol{\varepsilon}^{\mathrm{D}}$ is the vector of deviatoric strain components,

$$\boldsymbol{\varepsilon}^{\mathrm{D}} = \boldsymbol{\varepsilon} - \frac{\varepsilon_V}{3}\mathbf{I} \tag{12}$$

where ε_{V} is the volumetric strain,

$$\varepsilon_{\mathrm{V}} = \begin{cases} (\varepsilon_{xx} + \varepsilon_{yy}) & \text{for plane strain conditions} \\ \dfrac{1-2v}{1-v}(\varepsilon_{xx} + \varepsilon_{yy}) & \text{for plane stress conditions} \end{cases} \tag{13}$$

The pressure in the body is

$$p = -\kappa\varepsilon_{\mathrm{V}} \tag{14}$$

where the bulk modulus κ is

$$\kappa = \frac{E}{3(1-2v)} \tag{15}$$

In addition, we note that the vector of deviatoric stresses

$$\boldsymbol{\tau}^{\mathrm{D}} = \boldsymbol{\tau} + p\mathbf{I} \tag{16}$$

is related to vector of deviatoric strains by the following constitutive relationship:

$$\boldsymbol{\tau}^{\mathrm{D}} = \mathbf{C}^{\mathrm{D}}\boldsymbol{\varepsilon}^{\mathrm{D}} \tag{17}$$

Copyright © 2001 John Wiley & Sons, Ltd.

3.2. Variational form

We consider the following variational indicator [2]:

$$\Pi^*(\mathbf{u},p)=\int_\Omega\left[\frac{1}{2}\boldsymbol{\varepsilon}^{\mathrm{D}^{\mathrm{T}}}(\mathbf{u})\mathbf{C}^{\mathrm{D}}\boldsymbol{\varepsilon}^{\mathrm{D}}(\mathbf{u})-\frac{1}{2}\frac{p^2}{\kappa}-p\varepsilon_{\mathrm{V}}(\mathbf{u})\right]\mathrm{d}\Omega-\Re \tag{18}$$

The term $\Re$ accounts for the externally applied body forces, surface tractions and applied displacements,

$$\Re=\int_\Omega\mathbf{u}^{\mathrm{T}}\mathbf{f}^B\,\mathrm{d}\Omega+\int_{S_f}\mathbf{u}^{\mathrm{T}}\mathbf{f}^S\,\mathrm{d}S+\int_{S_u}\mathbf{f}^{u\mathrm{T}}(\mathbf{u}-\mathbf{u}^s)\,\mathrm{d}S \tag{19}$$

where $\mathbf{f}^u$ is the traction vector on the Dirichlet boundary S_u and may be expressed as

$$\mathbf{f}^u=\mathbf{N}\mathbf{C}^{\mathrm{D}}\boldsymbol{\varepsilon}^{\mathrm{D}}(\mathbf{u})-p\mathbf{N}\mathbf{I} \tag{20}$$

Here $\mathbf{f}^u$ is a vector of Lagrange multipliers to enforce the Dirichlet boundary conditions.

Invoking the stationarity of Π^* we obtain the following weak forms

$$\begin{aligned}&\int_\Omega\left[\boldsymbol{\varepsilon}^{\mathrm{DT}}(\mathbf{v})\mathbf{C}^{\mathrm{D}}\boldsymbol{\varepsilon}^{\mathrm{D}}(\mathbf{u})-\varepsilon_{\mathrm{V}}(\mathbf{v})p\right]\mathrm{d}\Omega-\int_{S_u}\left[\boldsymbol{\varepsilon}^{\mathrm{DT}}(\mathbf{v})\mathbf{C}^{\mathrm{D}}\mathbf{N}^{\mathrm{T}}\mathbf{u}+\mathbf{v}^{\mathrm{T}}\mathbf{N}\mathbf{C}^{\mathrm{D}}\boldsymbol{\varepsilon}^{\mathrm{D}}(\mathbf{u})\right]\mathrm{d}S+\int_{S_u}\mathbf{v}^{\mathrm{T}}\mathbf{N}\mathbf{I}\,p\,\mathrm{d}S\\&\quad=\int_\Omega\mathbf{v}^{\mathrm{T}}\mathbf{f}^B\,\mathrm{d}\Omega+\int_{S_f}\mathbf{v}^{\mathrm{T}}\mathbf{f}^S\,\mathrm{d}S-\int_{S_u}\boldsymbol{\varepsilon}^{\mathrm{D}^{\mathrm{T}}}(\mathbf{v})\mathbf{C}^{\mathrm{D}}\mathbf{N}^{\mathrm{T}}\mathbf{u}^S\,\mathrm{d}S\quad\forall\mathbf{v}\in H^1(\Omega)\end{aligned} \tag{21}$$

and

$$-\int_\Omega q\left[\varepsilon_{\mathrm{V}}(\mathbf{u})+\frac{p}{\kappa}\right]\mathrm{d}\Omega+\int_{S_u}q\mathbf{I}^{\mathrm{T}}\mathbf{N}^{\mathrm{T}}\mathbf{u}\,\mathrm{d}S=\int_{S_u}q\mathbf{I}^{\mathrm{T}}\mathbf{N}^{\mathrm{T}}\mathbf{u}^S\,\mathrm{d}S\quad\forall q\in L^2(\Omega) \tag{22}$$

where and $H^1(\Omega)$ and $L^2(\Omega)$ are the first-order Hilbert space and Lebesgue space of square integrable functions, respectively.

3.3. Nodal interpolations

We have the following approximation for the displacement field:

$$\mathbf{u}(x,y)=\sum_{J=1}^{N}\sum_{n\in\mathscr{I}}\mathbf{H}_{Jn}(x,y)\boldsymbol{\alpha}_{Jn}=\mathbf{H}(x,y)\mathbf{U} \tag{23}$$

where $\mathbf{U}=[\boldsymbol{\alpha}_{10}\ \boldsymbol{\alpha}_{11}\ \boldsymbol{\alpha}_{12}\ \ldots\ \boldsymbol{\alpha}_{Jn}\ \ldots]^{\mathrm{T}}$ is the vector of nodal unknowns and $\boldsymbol{\alpha}_{Jn}=[u^{Jn}\ v^{Jn}]$ is the vector of nodal unknowns at node J corresponding to the nth degree of freedom (u^{Jn} and v^{Jn} are the nodal variables for the x and y direction displacements at node J corresponding to the nth degree of freedom). The shape function matrix corresponding to node J and the nth degree of freedom is

$$\mathbf{H}_{Jn}(x,y)=\begin{bmatrix}h_{Jn}(x,y) & 0\\ 0 & h_{Jn}(x,y)\end{bmatrix}$$

Copyright © 2001 John Wiley & Sons, Ltd.

We choose the following approximation for the pressure field:

$$p(x,y)=\sum_{J=1}^{N}\sum_{n\in\mathscr{J}}h_{Jn}^{p}(x,y)\,p_{Jn}=\mathbf{H}_{p}(x,y)\mathbf{P} \tag{24}$$

where $\mathbf{P}=[p_{10}\ \ p_{11}\ \ p_{12}\ \ \ldots\ \ p_{Jn}\ \ \ldots]^{\mathrm{T}}$ is the vector of nodal point unknowns corresponding to the pressure degrees of freedom. The shape function $h_{Jn}^{p}(x,y)$ at node J corresponding to the nth degree of freedom is also generated using the partition of unity paradigm described in Section 2. This construction of the pressure approximation space results in a continuous pressure field.

The approximations for the strains in Equations (12) and (13) are

$$\boldsymbol{\varepsilon}^{\mathrm{D}}(x,y)=\sum_{J=1}^{N}\sum_{n\in\mathscr{J}}\mathbf{B}_{Jn}^{\mathrm{D}}(x,y)\boldsymbol{\alpha}_{Jn}=\mathbf{B}^{\mathrm{D}}(x,y)\mathbf{U} \tag{25}$$

and

$$\varepsilon_{\mathrm{V}}(x,y)=\mathbf{B}_{\mathrm{V}}(x,y)\mathbf{U} \tag{26}$$

where $\mathbf{B}^{\mathrm{D}}$ and $\mathbf{B}_{\mathrm{V}}$ are the corresponding strain interpolation matrices.

3.4. Discrete equations

Using Equations (23)–(26) in Equations (21) and (22) we obtain the following discrete sets of equations corresponding to node I and degree of freedom m:

$$\sum_{J=1}^{N}\sum_{n\in\mathscr{J}}\begin{bmatrix}\mathbf{K}_{uu_{Im,Jn}} & \mathbf{K}_{up_{Im,Jn}}\\ \mathbf{K}_{up_{Im,Jn}}^{\mathrm{T}} & \mathbf{K}_{pp_{Im,Jn}}\end{bmatrix}\begin{Bmatrix}\boldsymbol{\alpha}_{Jn}\\ p_{Jn}\end{Bmatrix}=\begin{Bmatrix}\mathbf{f}_{Im}\\ \mathbf{0}\end{Bmatrix}+\hat{\mathbf{f}}_{Im} \tag{27}$$

where

$$\mathbf{K}_{uu_{Im,Jn}}=\int_{\Omega_I}\mathbf{B}_{Im}^{\mathrm{DT}}\mathbf{C}^{\mathrm{D}}\mathbf{B}_{Jn}^{\mathrm{D}}\,\mathrm{d}\Omega \tag{28}$$

$$\mathbf{K}_{up_{Im,Jn}}=-\int_{\Omega_I}\mathbf{B}_{VIm}^{\mathrm{T}}h_{Jn}^{p}\,\mathrm{d}\Omega \tag{29}$$

$$\mathbf{K}_{pp_{Im,Jn}}=-\frac{1}{\kappa}\int_{\Omega_I}h_{Im}^{p}h_{Jn}^{p}\,\mathrm{d}\Omega \tag{30}$$

and

$$\mathbf{f}_{Im}=\int_{\Omega_I}\mathbf{H}_{Im}\mathbf{f}^{B}\,\mathrm{d}\Omega \tag{31}$$

where $\Omega_I=\Omega\cap B(\mathbf{x}_I,r_I)$. If I is a node associated with an 'interior sphere', then

$$\hat{\mathbf{f}}_{Im}=\mathbf{0}$$

from the property of compact support. If I is a node associated with a 'boundary sphere' then $\hat{\mathbf{f}}_{Im}$ allows us to incorporate the prescribed boundary conditions.

Copyright © 2001 John Wiley & Sons, Ltd.

If the sphere corresponding to node I has a non-zero intercept on the Neumann boundary S_f, then

$$\hat{\mathbf{f}}_{Im} = \begin{Bmatrix} \int_{S_{f_I}} \mathbf{H}_{Im} \mathbf{f}^S \, \mathrm{d}S \\ \mathbf{0} \end{Bmatrix} \tag{32}$$

where $S_f = \cup_{I \in \mathcal{N}_f} S_{f_I}$; $\mathcal{N}_f$ being the index set of such nodes.

On the other hand, if the sphere corresponding to node I has a non-zero intercept on the Dirichlet boundary S_u, then

$$\hat{\mathbf{f}}_{Im} = \sum_{J=1}^{N} \sum_{n \in \mathcal{I}} \begin{bmatrix} \mathbf{KU}_{uu_{Im\,Jn}} & \mathbf{KU}_{up_{Im\,Jn}} \\ \mathbf{KU}^{\mathrm{T}}_{up_{Im\,Jn}} & \mathbf{0} \end{bmatrix} \begin{Bmatrix} \boldsymbol{\alpha}_{Jn} \\ p_{Jn} \end{Bmatrix} - \begin{Bmatrix} \mathbf{fU}_{u_{Im}} \\ \mathbf{fU}_{p_{Im}} \end{Bmatrix} \tag{33}$$

where

$$\mathbf{KU}_{uu_{Im\,Jn}} = \int_{S_{u_I}} \mathbf{H}_{Im} \mathbf{N} \mathbf{C}^{\mathrm{D}} \mathbf{B}^{\mathrm{D}}_{Jn} \, \mathrm{d}S + \int_{S_{u_I}} \mathbf{B}^{\mathrm{DT}}_{Im} \mathbf{C}^{\mathrm{D}} \mathbf{N}^{\mathrm{T}} \mathbf{H}_{Jn} \, \mathrm{d}S \tag{34}$$

$$\mathbf{KU}_{up_{Im\,Jn}} = -\int_{S_{u_I}} \mathbf{H}_{Im} \mathbf{N} \mathbf{I} h^p_{Jn} \, \mathrm{d}S \tag{35}$$

$$\mathbf{fU}_{u_{Im}} = \int_{S_{u_I}} \mathbf{B}^{\mathrm{DT}}_{Im} \mathbf{C}^{\mathrm{D}} \mathbf{N}^{\mathrm{T}} \mathbf{u}^S \, \mathrm{d}S \tag{36}$$

and

$$\mathbf{fU}_{p_{Im}} = -\int_{S_{u_I}} h^p_{Im} \mathbf{I}^{\mathrm{T}} \mathbf{N}^{\mathrm{T}} \mathbf{u}^S \, \mathrm{d}S \tag{37}$$

where $S_u = \bigcup_{I \in \mathcal{N}_u} S_{u_I}$; $\mathcal{N}_u$ being the index set of such nodes.

A point to note is that we can incorporate the Dirichlet conditions exactly at nodes on the Dirichlet boundary by a special arrangement of the nodes [1].

4. NUMERICAL INTEGRATION ISSUES

Much of the computational effort in the method of finite spheres is expended on the accurate evaluation of the integrals presented in Section 3. One of the primary reasons for the success of the finite element technique is the ease with which numerical integration can be performed. The functions to be integrated are usually polynomials (or mapped polynomials), the elements do not overlap and they can be mapped to n-dimensional cubes. Hence Gauss–Legendre product rules are used for numerical integration with relatively low computational cost and high accuracy.

In the method of finite spheres, however, the shape functions are rational (nonpolynomial) functions and the integration domains are spheres, spherical shells or general sectors. Moreover, the spheres overlap giving rise to general lens-shaped regions. Hence, a separate class of integration rules is required.

Copyright © 2001 John Wiley & Sons, Ltd.

In this section, we focus on developing numerical integration rules for two-dimensional integration domains in the method of finite spheres. First, we recapitulate some of the rules presented in Reference [1] for integration on interior disks and boundary disks. We realize that integration on the lens shaped region of overlap of two disks is an important issue and propose and compare two different integration rules.

With the improvements in numerical integration reported in this section and the choice of the interpolation functions (see Section 3) the method of finite spheres was found to be about five times slower than the traditional finite element schemes when used to solve some representative test examples in 2D.

4.1. Integration on an interior disk

In this section we state a product cubature rule for the integral

$$\iint_{\Omega} f(x, y)\,\mathrm{d}x\,\mathrm{d}y \doteq \sum_i \sum_j D_{ij} f(x_i, y_j) \tag{38}$$

with an accuracy of k. The region, Ω, under consideration is a disk with radius R_0 (see Figure 2). The dot over the equality signifies that the relationship is a strict equality if the function $f(x, y)$ is a polynomial of order at most k in x and y, otherwise it is an approximation. The following theorem is due to Peirce [17].

Theorem 4.1. If it is required that the rule in Equation (38) have accuracy $k = 4m + 3$, $m = 0, 1, 2, \ldots$, in $x = r\cos\theta$ and $y = r\sin\theta$, and if it is required to have a minimum number of evaluation points which are taken at the intersection of concentric arcs (radius r_j) with rays emanating from the origin (angle θ_i), then it is both necessary and sufficient for the existence of a unique set of weights $D_{ij} \in R$ that

$$\theta_{i+1} - \theta_i = \frac{2\pi}{k+1}, \quad i = 1, 2, \ldots, k$$

and that the r_i^2 be the $m + 1$ zeros of $P_{m+1}(r^2)$, the Legendre polynomial in r^2 of degree $m + 1$, orthogonalized on $[0, R_0^2]$. The (unique) weights D_{ij} are of the form $A_i B_j$, where

$$A_i = \frac{2\pi}{k+1}, \quad i = 1, 2, \ldots, k+1$$

and

$$B_j = \frac{1}{2P'_{m+1}(r_j^2)} \int_0^{R_0^2} \frac{P_{m+1}(r^2)}{r^2 - r_j^2}\,\mathrm{d}r^2, \quad j = 1, 2, \ldots, m+1$$

For an interior disk (see Figure 2(a)), we use this theorem and are able to integrate with any given precision. The integration points are on equally spaced radii and the integration weights are independent of angular position (Gauss–Chebyshev rule in the θ-direction).

To demonstrate the efficiency of this rule we compare it with the Gauss–Legendre product rule on the disk

$$\iint_{\Omega} f(x, y)\mathrm{d}x\,\mathrm{d}y = \int_{y=-R_0}^{R_0} \int_{x=-X(y)}^{X(y)} f(x, y)\mathrm{d}x\,\mathrm{d}y \simeq \sum_{i=1}^{N_x} \sum_{j=1}^{N_y} D_{ij} f(x_i, y_j) \tag{39}$$

Copyright © 2001 John Wiley & Sons, Ltd.

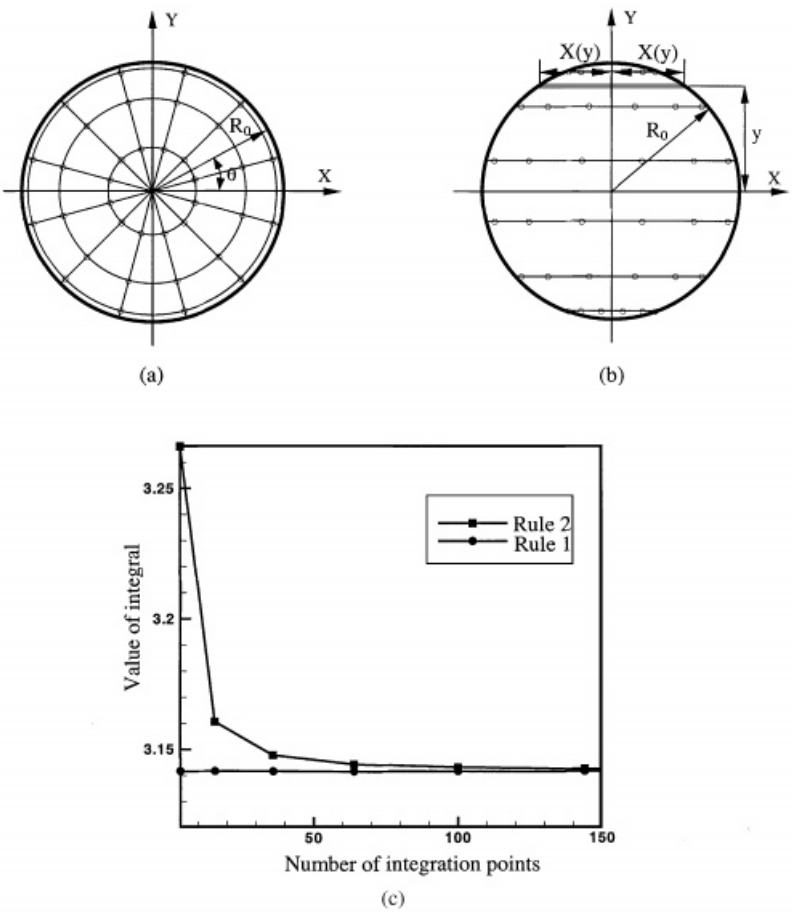

Figure 2. Integration on an 'interior' disk of radius 1.0. In (a) integration points corresponding to the rule in Theorem 4.1 (Rule 1) are shown. To integrate a polynomial of degree 11 exactly 36 integration points are required. In (b) integration stations corresponding to a Gauss–Legendre product rule (Rule 2) are shown. In (c) Rules 1 and 2 are used to evaluate the area of the disk.

where N_x and N_y are the number of integration points chosen along the x and y-directions, respectively, and $D_{ij} = W_i^x W_j^y$ is the product of the usual Gaussian weights W_i^x and W_j^y in the x and y-directions. It is not possible to guarantee exact integration of polynomials of any degree using this rule. For demonstration we consider the simple problem of computing the area of a unit circle (where $f(x, y) = 1$) in Figure 2(c).

4.2. Integration on a boundary sector

We categorize the boundary sectors into two major groups depending on the angle φ_0 that the radii joining the center of the disk to the two intercepts of the disk on S make interior to the domain:

Type I sector: $\varphi_0 \leqslant \pi$ (see Figure 3(a)). The rule that allows us to perform numerical cubature on this sector to any desired order of accuracy is computationally expensive [1].

Copyright © 2001 John Wiley & Sons, Ltd.

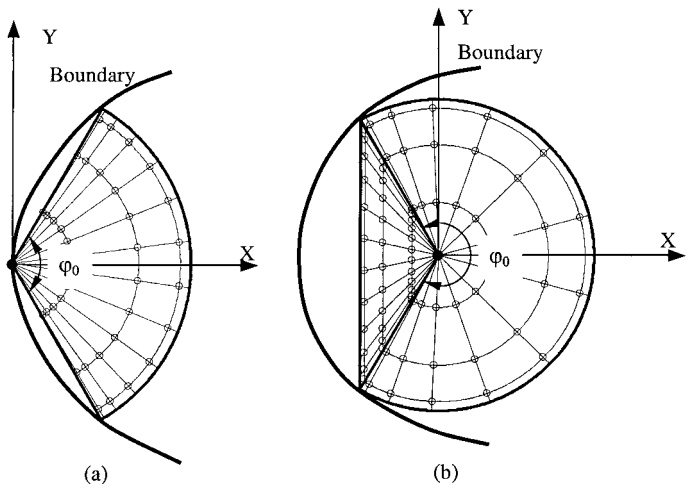

Figure 3. Integration points on a boundary sector: (a) type I boundary sector with $\varphi_0 \leqslant \pi$; (b) type II boundary sector with $\varphi_0 > \pi$.

We, therefore, propose an 'engineering solution' and use Gauss–Legendre quadrature in the θ-direction.

Type II sector: $\varphi_0 > \pi$ (see Figure 3(b)). This type of boundary sector is more expensive to handle. We decompose a Type II sector into a sector for which the rules of the Type I sector can be used and a triangle as shown in Figure 3(b). For the triangle we use a product rule based on Gauss–Legendre quadrature.

4.3. Integration on the lens

If nodes I and J are such that $B(\mathbf{x}_I, r_I) \cap B(\mathbf{x}_J, r_J) \neq 0$, then we propose two schemes for numerically evaluating $\iint_{\Omega_{IJ}} f(x, y)\mathrm{d}x\,\mathrm{d}y$ where $\Omega_{IJ} = B(\mathbf{x}_I, r_I) \cap B(\mathbf{x}_J, r_J)$:

Scheme 1 (see Figure 4(a)). In this scheme we use a Gauss–Legendre product rule of the form

$$\iint_{\Omega_{IJ}} f(x, y)\mathrm{d}x\,\mathrm{d}y = \int_{y=-y_0}^{y_0} \int_{x=-X_1(y)}^{X_2(y)} f(x, y)\,\mathrm{d}x\,\mathrm{d}y \simeq \sum_{i=1}^{N_x} \sum_{j=1}^{N_y} D_{ij} f(x_i, y_j) \tag{40}$$

where N_x and N_y are the number of integration points chosen along the x and y-directions, respectively and $D_{ij} = W_i^x W_j^y$ is the product of the usual Gaussian weights W_i^x and W_j^y in the x and y-directions.

Scheme 2 (see Figure 4(b)). In this scheme, we map the domain Ω_{IJ} onto a unit disk and compute the resulting integral using the scheme in Theorem 4.1

$$\iint_{\Omega_{IJ}} f(x, y)\mathrm{d}x\,\mathrm{d}y = \int_{\rho=0}^{1} \int_{\theta=0}^{2\pi} F(\rho, \theta) J\,\rho\,\mathrm{d}\rho\,\mathrm{d}\theta \tag{41}$$

where J is the Jacobian of the transformation.

Copyright © 2001 John Wiley & Sons, Ltd.

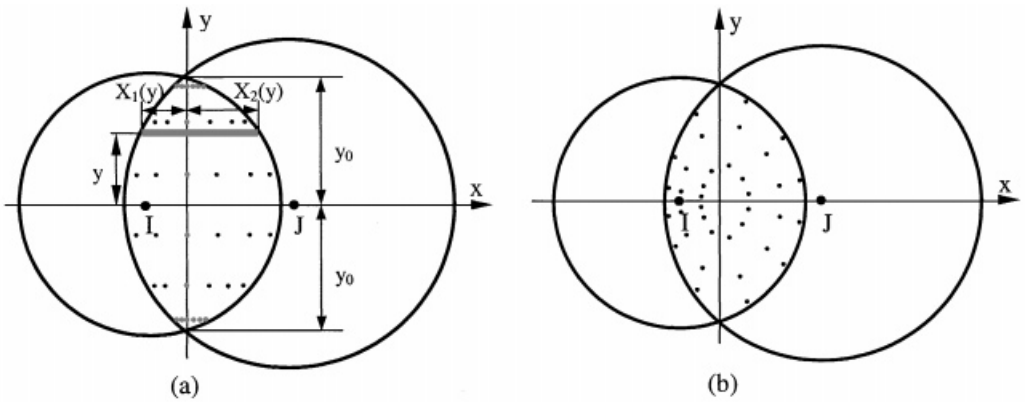

Figure 4. Integration on the lens. Some integration points generated using schemes 1, see (a) and 2, see (b), of Section 4.3 are shown on the intersection of two disks of radii 0.8 and 1.0, respectively, with centre-to-centre distance of 0.9.

We note that none of the schemes can guarantee polynomial accuracy for the integrand $f(x, y)$. However, numerical experiments performed using these two schemes suggest that scheme 1 requires fewer integration points for the same accuracy than scheme 2 [18].

5. INF–SUP TEST

In this section, we investigate the stability and optimality of the mixed formulation.

5.1. The inf–sup condition

To obtain a stable and optimal procedure for the selected interpolations, the mixed formulation in Equations (21) and (22) should satisfy the ellipticity condition (readily satisfied in this linear analysis since no reduced integration is used) and the inf–sup condition [2, 3]

$$\inf_{q_h \in Q_h} \sup_{\mathbf{v}_h \in V_h} \frac{\int_\Omega q_h \operatorname{div} \mathbf{v}_h \, \mathrm{d}\Omega}{\|q_h\|_0 \|\mathbf{v}_h\|_1} = \gamma_h \geqslant \gamma > 0 \tag{42}$$

where γ is a positive constant independent of h. $V_h \subset H_0^1(\Omega)$ is the displacement approximation space (H_0^1 contains functions that are in the first-order Hilbert space and satisfy the homogeneous Dirichlet boundary conditions of the problem) and Q_h is the pressure approximation space. The norms $\|\cdot\|_0$ and $\|\cdot\|_1$ are defined as

$$\|\cdot\|_0^2 = \int_\Omega (\cdot)^2 \, \mathrm{d}\Omega \tag{43}$$

and

$$\|\cdot\|_1^2 = \int_\Omega \sum_{i,j=1}^{2} \left(\frac{\partial (\cdot)_i}{\partial x_j} \right)^2 \mathrm{d}\Omega \tag{44}$$

Note that loading does not enter the inf–sup condition.

Copyright © 2001 John Wiley & Sons, Ltd.

5.2. Numerical inf–sup test

While it is highly desirable to obtain an analytical proof that a given discretization scheme satisfies the inf–sup condition (42), such proofs are quite difficult due to the complex (rational) nature of the interpolation functions used in the method of finite spheres. Hence, we adopt a numerical inf–sup test [2].

In the numerical inf–sup test, the inf–sup parameter γ_h in (42) is computed for a sequence of discretizations of a model problem. A mixed formulation with given displacement/pressure interpolations is said to have passed the inf–sup test if the inf–sup parameter asymptotically approaches a positive value greater than zero as the discretization is refined. Our experience is that if the inf–sup test is passed for a well-chosen problem, the inf–sup condition is satisfied.

In order to obtain the inf–sup parameter, γ_h, numerically for a given discretization, we express the relationship (42) in matrix form

$$\inf_{\mathbf{W}_h} \sup_{\mathbf{V}_h} \frac{\mathbf{W}_h^{\mathrm{T}} \mathbf{G}_h \mathbf{V}_h}{\sqrt{\mathbf{W}_h^{\mathrm{T}} \mathbf{G}_h \mathbf{W}_h} \sqrt{\mathbf{V}_h^{\mathrm{T}} \mathbf{S}_h \mathbf{V}_h}} = \gamma_h \geqslant \gamma > 0 \tag{45}$$

where

$$\|q_h\|_0^2 = \mathbf{W}_h^{\mathrm{T}} \mathbf{G}_h \mathbf{W}_h \tag{46}$$

and

$$\|\mathbf{v}_h\|_1^2 = \mathbf{V}_h^{\mathrm{T}} \mathbf{S}_h \mathbf{V}_h \tag{47}$$

We consider a sequence of discretizations in which all the displacement degrees of freedom corresponding to spheres that have nonzero intercepts with the Dirichlet boundary are set to zero. Then, for a given discretization, Equations (27) can be written as

$$\begin{bmatrix} (\mathbf{K}_{uu})_h & (\mathbf{K}_{up})_h \\ (\mathbf{K}_{up})_h^{\mathrm{T}} & -\frac{1}{\kappa}\mathbf{T}_h \end{bmatrix} \begin{Bmatrix} \mathbf{U}_h \\ \mathbf{P}_h \end{Bmatrix} = \begin{Bmatrix} \mathbf{f}_h \\ \mathbf{0} \end{Bmatrix} \tag{48}$$

where

$$\mathbf{T}_{h_{Im}Jn} = \int_{\Omega_I} h_{Im}^p h_{Jn}^p \, \mathrm{d}\Omega \tag{49}$$

We now consider the following generalized eigenvalue problem

$$\mathbf{G}_h' \boldsymbol{\psi}_h = \lambda \mathbf{T}_h \boldsymbol{\psi}_h \tag{50}$$

where

$$\mathbf{G}_h' = (\mathbf{K}_{up})_h^{\mathrm{T}} \mathbf{S}_h^{-1} (\mathbf{K}_{up})_h \tag{51}$$

If λ_p is the smallest eigenvalue of the generalized eigenvalue problem, then the inf–sup parameter is given by the relationship [2]

$$\gamma_h = \sqrt{\lambda_p} \tag{52}$$

Note that the rank verification test used by some researchers only addresses the issue of solvability and not of stability of the discretization scheme. For example, a scheme using

Copyright © 2001 John Wiley & Sons, Ltd.

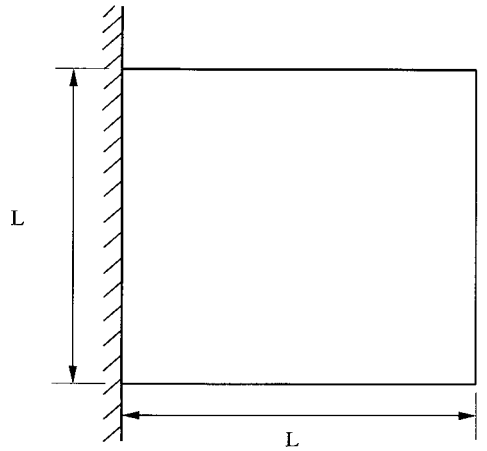

Figure 5. Problem considered for the inf–sup experiments: a cantilever plate ($L = 2.0$) in plane strain.

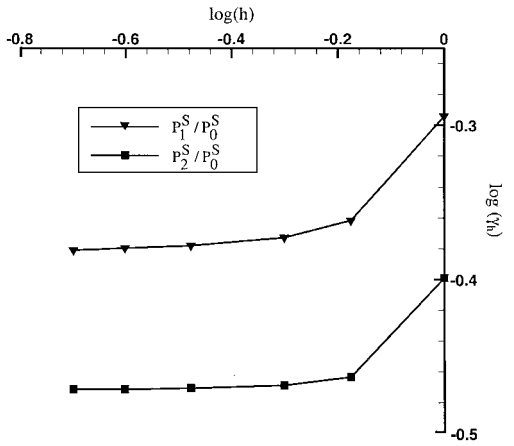

Figure 6. Inf–sup test results, P_1^S/P_0^S and P_2^S/P_0^S discretizations.

a first degree polynomial approximation for the displacement and pressure approximation spaces (number of displacement degrees of freedom per node $= 6$ and number of pressure degrees of freedom per node $= 3$, in R^2 for this case) passes the rank verification test but is unstable (see Section 5.3).

5.3. Results

In the finite element method, the inf–sup test described in Section 5.2 has been employed successfully in identifying specific displacement/pressure mixed interpolation schemes that are stable and result in optimal convergence [2]. We follow a similar approach in the context of the method of finite spheres and identify useful displacement/pressure interpolation schemes. The numerical scheme in Section 5.2 is used to test several discretizations in two-dimensional plane strain analysis.

Throughout the tests, the same system is used: the simple cantilevered square block, shown in Figure 5. This problem has been used to identify several effective finite element discretization schemes [2]. In every instance, the domain is discretized using a sequence of regular arrangement of nodes. The results are plotted in the form $\log(\gamma_h) = f(\log h)$, where γ_h is the inf–sup parameter in Equation (52) and h is the radius of each sphere.

In the finite element technique regular and irregular discretizations have been widely used for numerical inf–sup tests [2, 19]. However, in the method of finite spheres, the approximation space corresponding to a finer discretization does not contain the approximation space corresponding to a previous coarser discretization, and hence using even a regular grid is quite a severe test. But, of course, additional studies using irregular nodal arrangements would be valuable.

In order to satisfy the inf–sup condition (42), the inf–sup parameter must be bounded above zero with increase in refinement. Therefore, when a steady decrease of $\log(\gamma_h)$ is observed on the graph, the discretization scheme is said to fail the inf–sup test, whereas, if the inf–sup value approaches a value greater than zero with increase in refinement, the test is passed.

Copyright © 2001 John Wiley & Sons, Ltd.

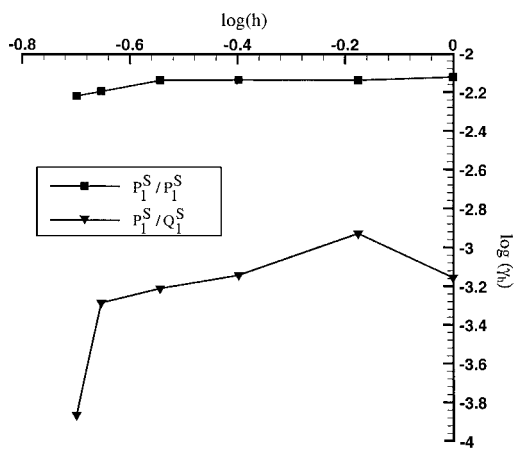

Figure 7. Inf–sup tests results, P_1^S/P_1^S and P_1^S/Q_1^S discretizations.

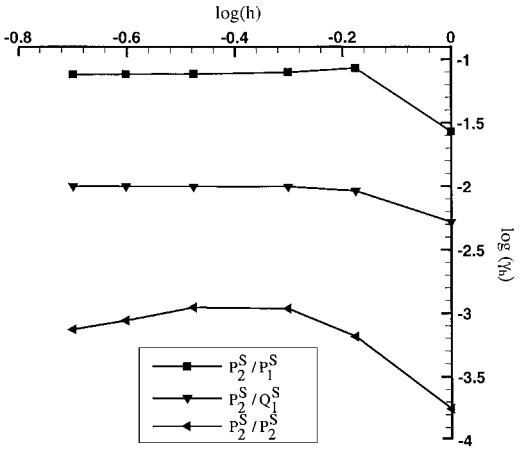

Figure 8. Inf–sup tests results, P_2^S/P_1^S, P_2^S/Q_1^S and P_2^S/P_2^S discretizations.

Table I. Inf–sup numerical predictions.

Discretization scheme	Numerical inf–sup prediction
P_1^S/P_0^S	PASS
P_1^S/P_1^S	FAIL
P_1^S/Q_1^S	FAIL
P_2^S/P_0^S	PASS
P_2^S/P_1^S	PASS
P_2^S/Q_1^S	PASS
P_2^S/P_2^S	FAIL

In this paper we focus attention on polynomial local approximation spaces. To label the various mixed interpolation function spaces we introduce the following notation. Let P_n and Q_n denote, respectively, the space of complete polynomials of degree 'n' and tensor product polynomials of degree 'n' in R^2 (e.g. $P_1 = \text{span}\{1, x, y\}$ and $Q_1 = \text{span}\{1, x, y, xy\}$). In the method of finite spheres we use the approximation spaces $P_n^S = \sum_{i=1}^N \varphi_i^0 P_n$ and $Q_n^S = \sum_{i=1}^N \varphi_i^0 Q_n$, and refer to a mixed interpolation scheme using, for example, P_n^S for displacement approximation and Q_n^S for the pressure approximation simply as the 'P_n^S/Q_n^S interpolation'.

We have considered seven different displacement/pressure discretization schemes. Figures 6–8 show the numerical results. The conclusions regarding whether the inf–sup test is passed or not are readily drawn and are summarized in Table I. It is interesting to observe that while the inf–sup parameter corresponding to certain discretizations that fail the inf–sup test (e.g. the P_1^S/P_1^S discretization) steadily decreases, the inf–sup parameter corresponding to certain other discretizations (e.g. the P_2^S/P_2^S discretization) initially increases and then starts

Copyright © 2001 John Wiley & Sons, Ltd.

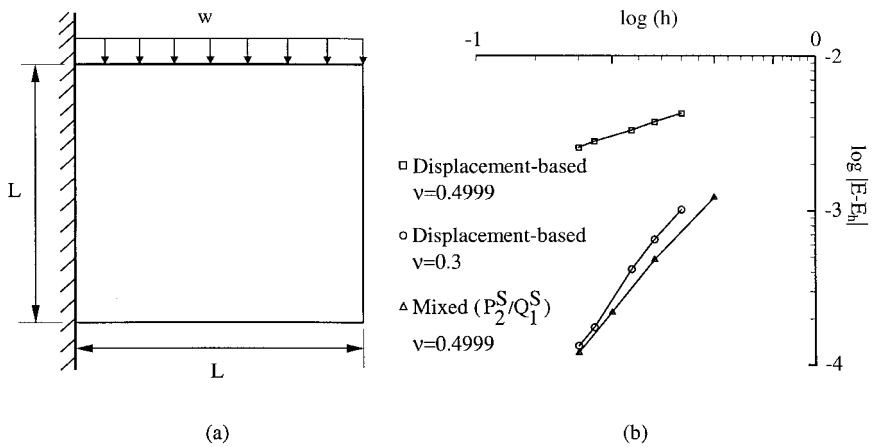

Figure 9. (a) Analysis of a cantilever plate ($L = 2.0$) in plane strain. Uniformly distributed load of magnitude $w = 1.0$ per unit length is applied. Poisson's ratio, $v = 0.3$ and 0.4999. In (b) the convergence in strain energy (E_h) with decrease in radius of support (h) is shown for two different Poisson ratios 0.3 and 0.4999. The pure displacement-based formulation is observed to lock when $v = 0.4999$. A mixed formulation using both pressure and displacement interpolations remedies locking (refer to the text for an explanation of the symbols used). E is an accurate estimate of the strain energy (reference solution).

to decrease. Another interesting point to note is that while in the finite element context, the simple 3/1 (P_1/P_0) element fails the inf–sup test, the P_1^S/P_0^S discretization scheme passes the test.

In Figure 9(b) we show the convergence in strain energy when a uniform h-type refinement is performed corresponding to two values of the Poisson ratio, v, equal to 0.3 and 0.4999. We observe that for the displacement-based method corresponding to the Poisson ratio of 0.3, we obtain an excellent convergence rate (as the discretization is refined). On the other hand, the displacement-based formulation 'locks' when the Poisson ratio is increased to 0.4999. The P_2^S/Q_1^S displacement/pressure mixed discretization scheme alleviates locking as expected (see Table I). The strain energy of the reference solution was obtained from a finite element analysis of the same problem using a 50×50 mesh of nine noded finite elements (9/3 displacement/pressure elements for the nearly incompressible case [2]).

Note that in none of the test cases zero eigenvalues were encountered indicating that no spurious pressure modes were present.

6. CONCLUDING REMARKS

In this paper we have developed a displacement/pressure mixed formulation to overcome the problem of 'locking' encountered in the pure displacement-based method of finite spheres. Several different discretization schemes have been tested for stability and optimal convergence properties using a numerical inf–sup test. All the discretization schemes considered in this paper assume continuous displacement and pressure fields. In this sense the formulation we have presented is analogous to the u/p-c formulation used in finite element analysis [2].

Copyright © 2001 John Wiley & Sons, Ltd.

An interesting observation is that the simple P_1^S/P_0^S discretization scheme passes the inf–sup test and is observed to be optimal. The variety in the behaviour of the inf–sup curves for the different discretization schemes is also noteworthy. While in this paper these curves have been used merely as indicators of whether a particular discretization scheme passes or fails the test, an analytical investigation regarding the behaviour of the inf–sup parameters would be very valuable.

The issue of computational efficiency is of utmost importance in determining the overall success of a meshless discretization scheme. We have focused our efforts to obtain a meshless scheme that is efficient and reliable. Computational efficiency is attained by use of a simple but efficient formulation and the proper choice of approximation functions and numerical integration schemes. In this paper, we have discussed several advances in these respects. We discuss the issues of efficiency in greater detail in a forthcoming publication [18].

REFERENCES

1. De S, Bathe KJ. The method of finite spheres. *Computational Mechanics* 2000; **25**:329–345.
2. Bathe KJ. *Finite Element Procedures*. Prentice-Hall: Englewood Cliffs, NJ, 1996.
3. Bathe KJ. The inf–sup condition and its evaluation for mixed finite element methods. *Computers and Structures* 2001; **79**:243–252.
4. Belytschko T, Lu YY, Gu L. Element free Galerkin methods. *International Journal for Numerical Methods in Engineering* 1994; **37**:229–256.
5. Lu YY, Belytschko T, Gu L. A new implementation of the element free Galerkin method. *Computer Methods in Applied Mechanics and Engineering* 1994; **113**:397–414.
6. Krysl P, Belytschko T. Analysis of thin shells by the element-free Galerkin method. *International Journal of Solids and Structures* 1996; **33**:3057–3080.
7. Zhu T, Atluri SN. A modified collocation method and a penalty formulation for enforcing the essential boundary conditions in the element free Galerkin method. *Computational Mechanics* 1998; **21**:211–222.
8. Askes H, de Borst R, Heeres O. Conditions for locking-free elasto-plastic analyses in the element-free Galerkin method. *Computer Methods in Applied Mechanics and Engineering* 1999; **173**:99–109.
9. Chen JS, Pan C, Wu CT. Large deformation analysis of rubber based on a reproducing kernel particle method. *Computational Mechanics* 1997; **19**:211–227.
10. Li S, Liu WK. Numerical simulations of strain localization in inelastic solids using meshfree methods. *International Journal for Numerical Methods in Engineering*, submitted.
11. Dolbow J, Belytschko T. Volumetric locking in the element free Galerkin method. *International Journal for Numerical Methods in Engineering* 1999; **46**:925–942.
12. Chen JS, Yoon S, Wang HP, Liu WK. An improved reproducing kernel particle method for nearly incompressible finite elasticity solids. *Computer Methods in Applied Mechanics and Engineering* 2000; **181**:117–145.
13. Chen JS, Wang HP, Yoon S, You Y. Some recent improvements in meshfree methods for incompressible finite elasticity boundary value problems with contact. *Computational Mechanics* 2000; **25**:137–156.
14. Duarte CA, Oden JT. *H–p* clouds—an *h–p* meshless method. *Numerical Methods in Partial Differential Equations* 1996; **12**:673–705.
15. Melenk JM, Babuška I. The partition of unity finite element method: basic theory and applications. *Computer Methods in Applied Mechanics and Engineering* 1996; **139**:289–314.
16. Shepard D. A two-dimensional interpolation function for irregularly spaced data. *Proceedings of 23rd National Conference on ACM* 1968; 517–524.
17. Peirce WH. Numerical integration over the planar annulus. *Journal of the Society for Industrial and Applied Mathematics* 1957; **5**(2):66–73.
18. De S, Bathe KJ. Towards an efficient meshless computational technique: the method of finite spheres. *Engineering Computations*, in press.
19. Iosilevich A, Bathe KJ, Brezzi F. On evaluating the inf–sup condition for plate bending elements. *International Journal for Numerical Methods in Engineering* 1997; **40**:3639–3663.

Copyright © 2001 John Wiley & Sons, Ltd.